Taylor & Francis
Taylor & Francis Group

The effects of radiometric terrain flattening on SAR-based forest mapping and classification

Alena Dostalova[a], Claudio Navacchi[a], Isabella Greimeister-Pfeil[a], David Small[b] and Wolfgang Wagner ![ORCID][a]

[a]Department of Geodesy and Geoinformation, Technische Universität Wien, Vienna, Austria; [b]Department of Geography, University of Zürich, Zürich, Switzerland

ABSTRACT

Terrain-induced variations of radar backscatter represent an important limiting factor of many Synthetic Aperture Radar (SAR)-based applications. Radiometric terrain flattening (RTF) is a well-established method that minimizes these variations in SAR imagery. To fully understand the implications of SAR RTF, validation of its impact on the derived products is needed. In this study, we quantified the influence of the RTF on a forest mapping and classification algorithm over Austria, and compared the classification results for the conventional sigma naught and radiometrically terrain-corrected gamma backscatter. The overall accuracy for forest/non-forest mapping and forest type classification improved by 2% and 4%, respectively, over the whole of Austria, with improvements of up to 16% and 20%, respectively, in regions with strong topography.

1. Introduction

Synthetic aperture radar (SAR) is an active microwave imaging system that allows to remotely map the reflectivity of objects or environments at microwave frequencies with high spatial resolution (Moreira 2013). SAR imagery is used in a wide range of applications that make use of the SAR normalized radar cross section (NRCS) that is represented in terms of a backscatter coefficient – an estimate of the backscatter per given reference area. Depending on which reference area convention is chosen for normalization, one can distinguish between three representations of the backscatter coefficient known as: i) beta naught (β^0), ii) sigma naught (σ^0) or iii) gamma naught (γ^0) (Small 2011). The σ^0 and γ^0 coefficients are normally calculated using an ellipsoid for the reference area computation and in this case, they have an important limitation, namely the fact that their radiometric properties are heavily distorted by topographic variations, even in only slightly undulating terrain. The topography-induced variations in SAR backscatter images are typically much larger than changes in backscatter coefficients due to the observed geophysical parameter (Atwood, Small, and Gens 2012; Villard and Le Toan 2014). As a result, SAR data are often discarded over hilly and mountainous areas.

CONTACT Alena Dostalova ✉ alena.dostalova@geo.tuwien.ac.at 🖃 Department of Geodesy and Geoinformation, Technische Universität Wien, Vienna, Austria

To overcome this limitation, several methods for the radiometric normalization of the backscatter coefficient were introduced in the literature. These include methods based on the local incidence angle (LIA) (Ulander 1996; Kellndorfer et al. 1998) or the actual ground area visible to the radar which is known as radiometric terrain flattening (RTF) (Small 2011). In recent years, the RTF became widely used, especially in snow or ice melt mapping (Scharien et al. 2017; Jewell et al. 2020) or forest monitoring (Rüetschi, Schaepman, and Small 2018; Akbari and Solberg 2020). The advantage of the RTF is evident mainly in areas with complex topography (Rüetschi, Schaepman, and Small 2018; Frey et al. 2012; Small et al. 2013; David et al. 2021), yet, to fully understand the benefit of this additional processing step, a validation of derived products with and without this step needs to be performed.

So far, only a limited number of studies quantified the influence of the RTF on the end product. Markert et al. (2020) evaluated the differences between two automated surface water mapping algorithms using the conventionally calibrated and radiometrically terrain flattened Sentinel-1 data as input for their algorithms. The authors found, that the algorithms using radiometrically terrain-flattened data as input yielded higher overall accuracies. These differences were, however, not significant. It should be noted that this analysis was limited to areas below 30 m in height relative to the nearest drainage as represented by the Height Above Nearest Drainage (HAND) index. This means that especially over scenes containing mountainous riverine, the HAND index mask might have masked considerable portions of terrain induced differences between the analysed datasets in case that they lie in high elevations relative to the drainage network. Atwood et al. (2014) analysed different approaches of topographic normalization including no correction (conventional approach), correction based on LIA, correction based on pixel area correction (RTF) and combination of the RTF correction with empirical slope normalization. They found that biomass estimates improved from no correction to LIA based corrections and further to the RTF and combined RTF and empirical slope corrections. This influence was shown to be smaller for estimates based solely on cross-polarization backscatter than for those based on co-polarized or dual-polarized data. After adaptation for polarimetric SAR data, the influence of the RTF for the land cover classification was assessed by Atwood, Small, and Gens (2012). The largest improvements were observed for the deciduous forest class, and the impact of the RTF step was highlighted by comparing the classification performed separately for regions facing towards and away from the satellite.

The reported benefits of RTF come at the cost of additional processing resources. Especially for large-scale applications the additional computational effort of the RTF may be large. Hence, it is essential to assess the potential of this additional processing step on the end product. In this study, we evaluated results of a forest mapping and forest type classification algorithm (Dostálová et al. 2021) using a standard, ellipsoid corrected σ_E^0 and the radiometrically terrain corrected γ_T^0 backscatter as an input over Austria. The improvements were quantified in respect to terrain slope and aspect in order to identify those regions, where this additional step provides highest improvements.

2. Study area and used data

2.1. Study area

Our study area is Austria where 62% of the land area is covered by Alps. The north-eastern parts are dominated by flatlands with elevations between 120 and 300 m a.s.l., while central and western parts of Austria are covered by alpine terrain with many peaks exceeding 3000 m a.s.l. As such, it represents an ideal test area for the influence of radiometric terrain flattening. The study area is shown in Figure 1.

3. Used data

3.1. Sentinel-1

For the purpose of this study, all available Sentinel-1 Ground Range Detected (GRD) Interferometric Wide (IW) swath mode acquisitions from year 2017 for the whole of Austria were used. The preprocessed data were available via the Austrian Data Cube (ACube, (EODC 2018)). The pre-processing steps for the σ_E^0 images included precise orbit correction, border noise removal, radiometric correction to σ_E^0 and orthorectification using the Range-Doppler terrain correction (Small and Schubert 2008) method. For γ_T^0, precise orbit correction, border noise removal, radiometric correction to the (β^0) values, radiometric terrain flattening and Range-Doppler terrain correction were applied. A terrain model based on airborne laser scanning (Geoland 2020) resampled onto 10 m grid was used for the radiometric terrain flattening and the Range-Doppler terrain correction steps.

3.2. Reference data

For the validation of the forest/non-forest classification, a 1 m forest/non-forest map based on aerial imagery and ALS data provided by the Austrian Research Centre for Forests (BFW) was used. It was resampled to the 10 m sample interval such that a pixel was assigned to the forest class in cases when 25% of all 1 m pixels within the 10 m pixel were classified as forests. For the forest type validation, the Copernicus High Resolution Layers (HRL) 2018 10 m Dominant Leaf Type was used (EEA 2021). This forest type map contains
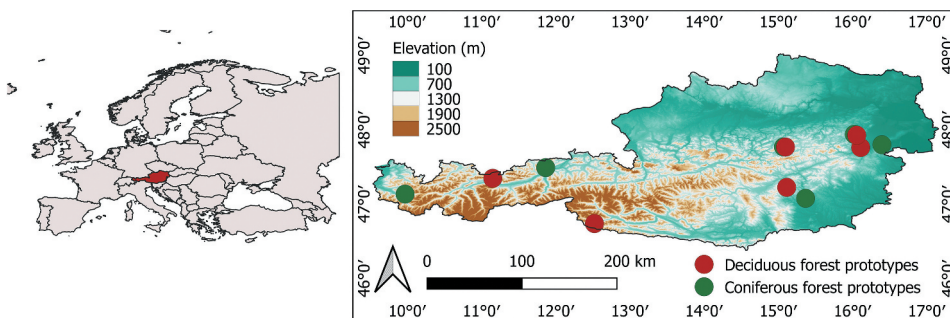

Figure 1. Overview of the study area (Austria) with the locations of the signature prototypes for the forest type classification overlaid on the terrain model of Austria based on airborne laser scanning.

three classes (no forest, coniferous and broadleaf forest) and, according to the internal validation (EEA 2021), the users and producers accuracy of each class exceeds 90% with an overall accuracy of 96.5%.

4. Methodology

The forest mapping and classification algorithm (Dostálová et al. 2021) uses either σ_E^0 or γ_T^0 backscatter as input, while the rest of the processing steps (i.e., SAR seasonality time series computation and construction of the forest maps) remain the same. A brief description of the main steps is provided in the following subsections, and details can be found in Dostálová et al. (2021, 2018).

4.1. SAR seasonality time series computation

The forest mapping and classification algorithm (Dostálová et al. 2021) uses as input 1 year of Sentinel-1 measurements. Due to the varying coverage patterns, changing acquisition geometry and environmental conditions of the individual acquisitions, several steps are applied to minimize the quickly varying conditions (such as the influence of the varying incidence angle of the SAR signal or changes in surface and vegetation moisture content) and derive time series with time step of 12 days. First, a normalization to a common reference angle was applied using the slope (β) parameter. This correction is applied to minimize the effect of the varying sensor-target geometry in order to combine the acquisitions taken from several relative orbits (Peters et al. 2012). The slope parameter is computed using a linear regression between the backscatter coefficient (in dB) and projected local incidence angle (θ) values. It is computed separately for each image pixel and uses the full time-series of all available Sentinel-1 acquisitions from 2017. The normalization equations for σ_E^0 and γ_T^0 backscatter read as follows:

$$\sigma_{E40}^0 = \sigma_E^0(\theta) - \beta(\theta - 40°) \tag{1}$$

$$\gamma_{T40}^0 = \gamma_T^0(\theta) - \beta(\theta - 40°) \tag{2}$$

Next, the mean of the normalized backscatter was computed using all available acquisitions covering each 12-day interval, and smoothed using a Gaussian temporal filter with std. dev. of 1 to smooth the signal variation caused by the quickly varying environmental conditions (such as changes in surface and vegetation moisture content or freeze/thaw effects). The resulting time series captures the annual variability of the signal, and reflects the seasonal changes of various vegetation types (Rüetschi, Schaepman, and Small 2018; Dostálová et al. 2018).

4.2. Construction of the forest map

The forest classification algorithm (Dostálová et al. 2021) exploits differences between the seasonality time series – temporal signatures – of various vegetation types. Signature prototypes are computed as described in the previous chapter using averaged backscatter values over 300 m × 300 m large forested areas (30 × 30 pixels) and are selected to

represent both coniferous and broadleaved forest types. The selection of the signature prototype locations was supported by reference datasets, orthophotos as well as average Sentinel-1 backscatter for 2017 to exclude areas with apparent terrain effects or clear cuts. The locations of the signature prototypes over Austria are shown in Figure 1.

The classification algorithm uses the similarity measures – Root Mean Square Difference (RMSD) and Pearson correlation coefficient (r) – between the prototype signatures and the respective temporal signature of each individual pixel. In the first step, forest/non-forest classes are assigned using thresholds: forest class is assigned in case that the vertical transmitted-horizontal recieved (VH) and vertical transmitted-vertical recieved (VV) polarization RMSD are below 1.5 dB and 2.0 dB, respectively, and VH polarization r exceeds 0.4. Consequently, the forest type (coniferous, broadleaf) is assigned to each forested pixel according to the lowest RMSD value in VH polarization. For the final forest type map, minimal mapping units (MMU) of 0.5 ha were applied. The forest type map has three classes: non-forest, coniferous forest and broadleaf forest.

4.3. Validation

σ_E^0- and γ_T^0-based forest maps were computed for the whole of Austria and compared to reference maps. The forest/non-forest accuracies were computed using all pixels. In case of the forest type dataset, pixels classified as non forest in Sentinel-1 forest maps or Copernicus HRL dominant leaf type map were excluded from the forest type classification. The focus of the validation was put on two aspects. First, the spatial distribution of differences between the σ_E^0 and γ_T^0 forest maps was highlighted by computing and plotting the validation statistics for 10 km large tiles as well as for entire validation area. Secondly, the influence of the local terrain aspect and slope on the map's accuracy was assessed by computing the validation statistics separately for several terrain slope and aspect intervals.

5. Results and discussion

5.1. Spatial overview

Spatial overviews of the forest mapping and classification results for γ_T^0 and σ_E^0 are shown in Figures 2 and 3, respectively. Each figure shows the reference map (BFW forest mask and Copernicus HRL Forest Type map for forest/non-forest and forest type map, respectively) together with the difference images between the reference map and the γ_T^0- and σ_E^0-based classification results and the spatial distribution of the difference between the overall accuracy of the γ_T^0 and σ_E^0 results.

For forest/non-forest mapping, distinct patterns are apparent in the maps showing the differences in classification and especially the classification accuracy improvements. It is apparent that the largest differences between the Sentinel-1 and reference forest maps are located in mountainous regions (see Figure 1). This was to be expected, and was already postulated in previous works (Dostálová et al. 2021, 2018). Also, the accuracy of the classification in mountainous areas improved the most when using γ_T^0 instead of σ_E^0 as an input for the classification algorithm – the improvements locally reached as high as 16% in the case of the forest/non-forest map. This is mainly due to the omission of the
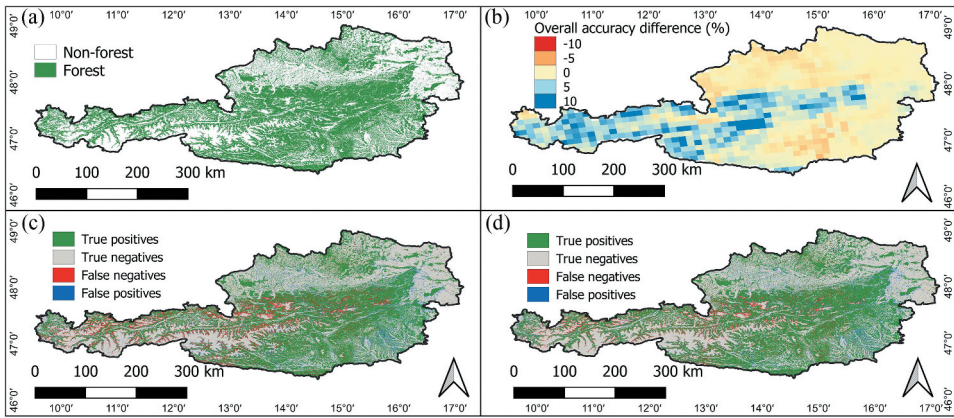
Figure 2. Overview of the results of the forest mapping algorithm. (a) Reference forest map from the Austrian Centre for Forests (BFW). (b) Difference between the overall accuracy of the γ^0_T and σ^0_E forest/non-forest map computed for 10 km large tiles. (c) Difference map between the σ^0_E Sentinel-1 and reference forest/non-forest map. (d) Difference map between the γ^0_T Sentinel-1 and reference forest/non-forest map.
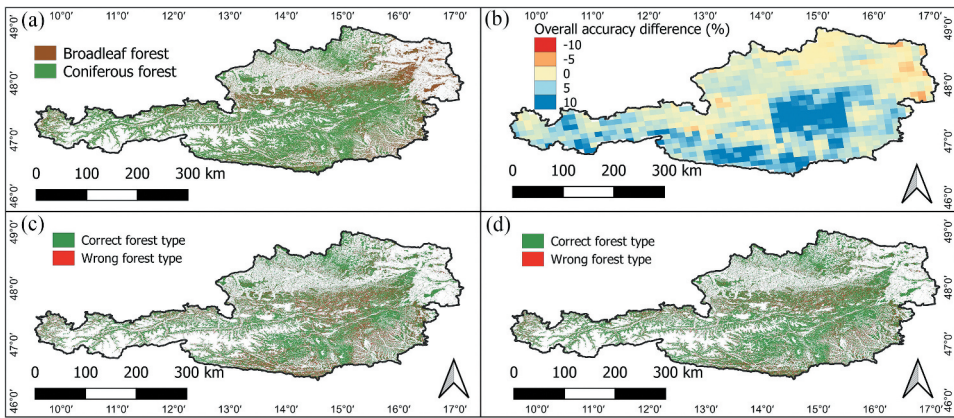

Figure 3. Overview of the results of the forest classification algorithm. (a) Reference forest map from Copernicus HRL. (b) Difference between the overall accuracy of the γ^0_T and σ^0_E forest type map computed for 10 km large tiles. (c) Difference map between the σ^0_E Sentinel-1 and reference forest type map. (d) Difference map between the γ^0_T Sentinel-1 and reference forest type map.

forest area in mountainous regions, where insufficient correction of the terrain effects hinders the classification. In the flatland, the overall accuracies of the γ^0_T and σ^0_E forest/non-forest maps are comparable except few areas located mainly in southern Austria where the γ^0_T-based forest map shows slightly increased commission error for forest class. As a result, the overall accuracy locally decreased, causing maximal differences of up to 3%.

In the case of forest type classification, the improvements were also mainly in mountainous regions. However, the pattern followed that of the terrain model less strictly. This is due to the fact that western Austria, where the highest improvements are observable

for forest/non-forest mapping, is dominated by coniferous forests while the broadleaf forests are very sparse. The classification accuracy improved the most in central and southern Austria, where the elevation ranges up to 2000 m a.s.l., but the portion of deciduous forest stands is relatively high. In these regions, the overall accuracy of the forest type classification locally increased by up to 20%. In the flatlands, the differences in the overall accuracies of the γ_T^0 and σ_E^0 forest type map varied by ±5%.

The overall accuracy as well as user's and producer's accuracies for each class over the whole of Austria for various local terrain slope ranges is summarized in Table 1. When computed over the entire range of the local terrain slopes, the overall accuracy improved by 2% from 87% to 89% in case of forest/non-forest classification and by 4% from 78% to 82% in case of forest type classification. Furthermore, the user's and producer's accuracies of all classes stayed the same or were improved.

5.2. Influence of terrain slope and aspect

With steeper local terrain slope, the difference between the ellipsoid-based reference area used for σ_E^0 and the reference area computed from the digital elevation model (DEM) for γ_T^0 increases. As a result, both maps differ more in areas with steep slopes. The influence of the local terrain slope on the overall accuracy of the forest/non-forest and forest type maps is demonstrated in Table 1.

In case of the forest type classification, the accuracies based on σ_E^0 and γ_T^0 are comparable for slopes up to 20°. With increasing terrain slope, the accuracies of the forest/non-forest map rapidly decrease in case of σ_E^0. This is mainly caused by high omission error of the forest class; for slopes between 40° and 50°, the producers' accuracy of the σ_E^0-based forest class is only 63% as compared to 75% in case of γ_T^0-based forest map. Overall, the

Table 1. Overall (OA), Producer's (PA) and User's (UA) accuracies (in percent) of the σ_E^0- and γ_T^0-forest /non-forest (F/NF) and forest type (Broadleaved – B or Coniferous – C) maps when compared to the BFW forest mask and Copernicus HRL dominant leaf type map, respectively, for various local terrain slope ranges.

	σ_E^0					γ_T^0				
	OA	PA		UA		OA	PA		UA	
Slope range (°)		F	NF	F	NF		F	NF	F	NF
Forest/non-forest										
0–90	87	84	90	89	86	89	87	91	90	88
0–10	92	92	92	80	97	92	92	92	80	97
10–20	89	90	86	90	86	89	90	86	90	86
20–30	86	86	86	94	72	88	88	88	95	76
30–40	78	74	88	93	59	85	83	91	96	69
40–50	73	63	89	90	60	81	75	92	94	69
50–70	73	51	89	78	71	78	61	91	84	76
Forest type		B	C	B	C		B	C	B	C
0–90	78	68	82	61	86	82	68	89	71	89
0–10	79	70	86	77	81	82	70	89	82	82
10–20	81	67	86	66	87	84	69	90	72	88
20–30	77	66	81	53	88	83	65	89	66	89
30–40	72	69	73	47	87	81	63	87	63	87
40–50	71	69	71	46	87	78	64	83	57	86
50–70	68	64	69	36	87	72	57	77	40	86

decrease in accuracies with steeper slope is slower for the γ_T^0-based forest/non-forest map. For instance, difference between the overall accuracy of σ_E^0 and γ_T^0 forest/non-forest classification for slopes between 40° and 50° reaches 8%. This shows, that by using the proper way to calculate the reference area in the radiometric correction step, a large portion of terrain induced errors can be eliminated. In case of the forest type classification, the overall accuracy is higher for all terrain slope ranges, even for slopes below 20°, where this difference is 3%.

For γ_T^0-based forest maps, large decrease of accuracies is visible for the slopes between 50° and 70°, especially for the producers' accuracy of the forest class and users' accuracy of the broadleaf forest class. We assume that for such steep slopes, the terrain distortions in SAR data become too large to be corrected by applying the RTF correction. Slopes above 70° are not shown due to a small number of available samples.

SAR backscatter is sensitive to the viewing geometry, which introduces errors to the classification algorithm and reduces its accuracy for slopes facing the sensor for either ascending or descending orbit. Figure 4 shows the forest/non-forest classification accuracy as a function of a local terrain aspect. It remains relatively stable in case of shallow slopes up to 20° (see Figure 4: left) and is not improved by including the RTF correction. In case of steep slopes between 40° and 50° (see Figure 4: right), the overall accuracy of the σ_E^0 based forest/non-forest classification varies between 62% and 85%, with lowest values for slopes facing the sensor for either ascending or descending orbit pass. This dependency on local terrain aspect is reduced but not removed by applying the RTF correction (the overall accuracies range between 72% and 87%).
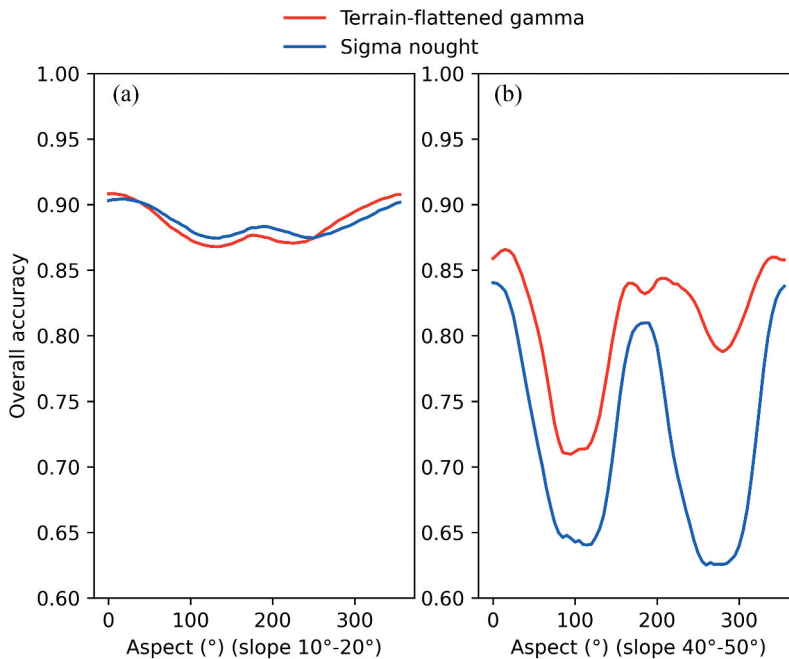

Figure 4. Dependency of overall accuracy of the forest/non-forest classification on the local terrain aspect. (a) Local terrain slope from 10° to 20°. (b) Local terrain slope from 40° to 50°.

6. Conclusion

Terrain-induced variations in the SAR backscatter are a limiting factor to many SAR applications. By replacing conventional ellipsoid-based radiometrically calibrated backscatter coefficients with radiometrically terrain-flattened and -corrected γ_T^0, we showed improvements in the data quality over undulated terrain. We quantified the effect of the RTF on the accuracy of forest mapping and classification algorithms over Austria. Significant improvements (16% and 20% for forest/non-forest mapping and forest type classification) were observed in highly undulated areas when γ_T^0 backscatter was used instead of σ_E^0. In flatlands, the forest/non-forest results remained comparable for both backscatter coefficient conventions while the forest type classification improved by 3% even for slopes below 10%. These results demonstrate the great benefit of the radiometric terrain flattening. While in flatlands, the results may remain comparable or slightly improve, in sloped terrain, application of the RTF correction strongly reduces classification errors.

Disclosure statement

The authors report there are no competing interests to declare.

ORCID

Wolfgang Wagner http://orcid.org/0000-0001-7704-6857

References

Akbari, V., and S. Solberg. 2020. "Clear-Cut Detection and Mapping Using Sentinel-1 Backscatter Coefficient and Short-Term Interferometric Coherence Time Series." *IEEE Geoscience and Remote Sensing Letters* 19: 1–5. doi:10.1109/LGRS.2020.3039875.
Atwood, D. K., D. Small, and R. Gens. 2012. "Improving PolSAR Land Cover Classification with Radiometric Correction of the Coherency Matrix." *IEEE Journal of Selected Topics in Applied Earth Observations and Remote Sensing* 5 (3): 848–856. doi:10.1109/JSTARS.2012.2186791.
Atwood, D. K., H.-E. Andersen, B. Matthiss, and F. Holecz. 2014. "Impact of Topographic Correction on Estimation of Above Ground Boreal Biomass Using Multi-Temporal, L-Band Backscatter." *IEEE Journal of Selected Topics in Applied Earth Observations and Remote Sensing* 7 (8): 3262–3273. doi:10.1109/JSTARS.2013.2289936.

David, S., C. Rohner, N. Miranda, M. Rüetschi, and M. E. Schaepman. 2021. "Wide-Area Analysis-Ready Radar Backscatter Composites." *IEEE Transactions on Geoscience and Remote Sensing* 60: 1–14.

Dostálová, A., W. Wagner, M. Milenković, and M. Hollaus. 2018. "Annual Seasonality in Sentinel-1 Signal for Forest Mapping and Forest Type Classification." *International Journal of Remote Sensing* 39 (21): 7738–7760. doi:10.1080/01431161.2018.1479788.

Dostálová, A., M. Lang, J. Ivanovs, L. T. Waser, and W. Wagner. 2021. "European Wide Forest Classification Based on Sentinel-1 Data." *Remote Sensing* 13 (3): 337. doi:10.3390/rs13030337.

EEA. 2021. "User Manual: Copernicus Land Monitoring Service, High Resolution Land Cover Characteristics, Tree-Cover/forest and Change 2015-2018." Accessed 4 February 2022. https://land.copernicus.eu/user-corner/technical-library/forest-2018-user-manual.pdf

EODC. 2018. "Acube. Austrian Data Cube. An EODC Service for the Austrian Earth Observation Community." Accessed 30 March 2021. https://acube.eodc.eu

Frey, O., M. Santoro, C. L. Werner, and U. Wegmuller. 2012. "DEM-Based SAR Pixel-Area Estimation for Enhanced Geocoding Refinement and Radiometric Normalization." *IEEE Geoscience and Remote Sensing Letters* 10 (1): 48–52. doi:10.1109/LGRS.2012.2192093.

Geoland. 2020. "Digitales Geländemodell (DGM) Österreich." Accessed 30 March 2021. https://www.data.gv.at/katalog/dataset/dgm

Jewell, L., R. R. Forster, S. B. Rupper, E. J. Deeb, H.P. Marshall, M. Zia Hashmi, and E. Burgess. 2020. "Mapping Snowmelt Progression in the Upper Indus Basin with Synthetic Aperture Radar." *Frontiers in Earth Science* 7: 318. doi:10.3389/feart.2019.00318.

Kellndorfer, J. M., L. E. Pierce, M. Craig Dobson, and F. T. Ulaby. 1998. "Toward Consistent Regional-To-Global-Scale Vegetation Characterization Using Orbital SAR Systems." *IEEE Transactions on Geoscience and Remote Sensing* 36 (5): 1396–1411. doi:10.1109/36.718844.

Markert, K. N., A. M. Markert, T. Mayer, C. Nauman, A. Haag, A. Poortinga, B. Bhandari, et al. 2020. "Comparing Sentinel-1 Surface Water Mapping Algorithms and Radiometric Terrain Correction Processing in Southeast Asia Utilizing Google Earth Engine." *Remote Sensing* 12 (15): 2469. doi:10.3390/rs12152469.

Moreira, A. 2013. "Synthetic Aperture Radar (SAR): Principles and Applications."

Peters, J., H. Lievens, B. De Baets, and N.E.C. Verhoest, N. E. C. Verhoest et al. 2012. "Accounting for Seasonality in a Soil Moisture Change Detection Algorithm for ASAR Wide Swath Time Series." *Hydrology and Earth System Sciences* 16 (3): 773–786. doi:10.5194/hess-16-773-2012.

Rüetschi, M., M. E. Schaepman, and D. Small. 2018. "Using Multitemporal Sentinel-1 C-Band Backscatter to Monitor Phenology and Classify Deciduous and Coniferous Forests in Northern Switzerland." *Remote Sensing* 10 (1): 55. doi:10.3390/rs10010055.

Scharien, R. K., R. Segal, S. Nasonova, V. Nandan, S. E. Howell, and C. Haas. 2017. "Winter Sentinel-1 Backscatter as a Predictor of Spring Arctic Sea Ice Melt Pond Fraction." *Geophysical Research Letters* 44 (24): 12–262. doi:10.1002/2017GL075547.

Small, D., and A. Schubert. 2008. "Guide to ASAR Geocoding." *ESA-ESRIN Technical Note RSL-ASAR-GC-AD* 1: 36.

Small, D. 2011. "Flattening Gamma: Radiometric Terrain Correction for SAR Imagery." *IEEE Transactions on Geoscience and Remote Sensing* 49 (8): 3081–3093. doi:10.1109/TGRS.2011.2120616.

Small, D., N. Miranda, T. Ewen, and T. Jonas. 2013. "Reliably Flattened Radar Backscatter for Wet Snow Mapping from Wide-Swath Sensors." *ESA-SP* 772 91. doi:10.5167/uzh-96170.

Ulander, L. M. 1996. "Radiometric Slope Correction of Synthetic-Aperture Radar Images." *IEEE Transactions on Geoscience and Remote Sensing* 34 (5): 1115–1122. doi:10.1109/36.536527.

Villard, L., and T. Le Toan. 2014. "Relating P-Band SAR Intensity to Biomass for Tropical Dense Forests in Hilly Terrain: Gamma0 or T0?" *IEEE Journal of Selected Topics in Applied Earth Observations and Remote Sensing* 8 (1): 214–223. doi:10.1109/JSTARS.2014.2359231.